

PREPARED FOR SUBMISSION TO JCAP

Limits on Non-Relativistic Matter During Big-Bang Nucleosynthesis

Tsung-Han Yeh,^{a,1} Keith A. Olive^b Brian D. Fields^{c,d,e}

^aTRIUMF, 4004 Wesbrook Mall, Vancouver, BC V6T 2A3, Canada

^bWilliam I. Fine Theoretical Physics Institute, School of Physics and Astronomy, University of Minnesota, Minneapolis, MN 55455

^cDepartment of Astronomy, University of Illinois, Urbana, IL 61801

^dDepartment of Physics, University of Illinois, Urbana IL 61801

^eIllinois Center for Advanced Studies of the Universe

E-mail: thyeh@triumf.ca

Abstract. Big-bang nucleosynthesis (BBN) probes the cosmic mass-energy density at temperatures ~ 10 MeV to ~ 100 keV. Here, we consider the effect of a cosmic matter-like species that is non-relativistic and pressureless during BBN. Such a component must decay; doing so during BBN can alter the baryon-to-photon ratio, η , and the effective number of neutrino species. We use light element abundances and the cosmic microwave background (CMB) constraints on η and N_ν to place constraints on such a matter component. We find that electromagnetic decays heat the photons relative to neutrinos, and thus dilute the effective number of relativistic species to $N_{\text{eff}} < 3$ for the case of three Standard Model neutrino species. Intriguingly, likelihood results based on *Planck* CMB data alone find $N_\nu = 2.800 \pm 0.294$, and when combined with standard BBN and the observations of D and ^4He give $N_\nu = 2.898 \pm 0.141$. While both results are consistent with the Standard Model, we find that a nonzero abundance of electromagnetically decaying matter gives a better fit to these results. Our best-fit results are for a matter species that decays entirely electromagnetically with a lifetime $\tau_X = 0.89$ sec and pre-decay density that is a fraction $\xi = (\rho_X/\rho_{\text{rad}})|_{10 \text{ MeV}} = 0.0026$ of the radiation energy density at 10 MeV; similarly good fits are found over a range where $\xi\tau_X^{1/2}$ is constant. On the other hand, decaying matter often spoils the BBN+CMB concordance, and we present limits in the (τ_X, ξ) plane for both electromagnetic and invisible decays. For dark (invisible) decays, standard BBN (i.e. $\xi = 0$) supplies the best fit. We end with a brief discussion of the impact of future measurements including CMB-S4.

¹Corresponding author.

Contents

1	Introduction	1
2	Formalism	3
3	Inputs: Light Element Abundances and the CMB	8
4	Results	10
4.1	Case (a): Electromagnetic Decays	13
4.2	Case (b): Invisible decays	16
5	Discussion	18

1 Introduction

The successful concordance between big bang nucleosynthesis (BBN) [1–9], the observational determination of the light elements D/H [10–17], and ^4He [18–23], and observations of the cosmic microwave background (CMB) anisotropies [24, 25] is one of the foundations of early universe big bang cosmology. BBN is sensitive to all four fundamental forces, and to any cosmic effects that can change the expansion rate. As a result it opens a window to new physics, probing new cosmic components present in the first seconds to minutes at a temperature scale between 10 keV and 10 MeV. As such, it provides one of the deepest probes into the Universe which is based on 1) known physics, and 2) observations. Its success using Standard Model inputs (of cosmology and nuclear and particle physics), allows for very little deviation from the Standard Model and as such it is possible to place strong constraints on physics beyond the Standard model which is effective at temperatures around 1 MeV [26–31]. These include dark matter and dark energy, as well as new forms of radiation. Most notable among these is the limit on the number of relativistic degrees of freedom present during BBN, often parameterized by the number of neutrino flavors. In a recent analysis this was found to be $N_\nu < 3.180$ (95 % CL) [31].

While additional relativistic degrees of freedom contribute to the total energy density, and speed-up the expansion of the Universe, they do not change the equation of state. In many theories of physics beyond the Standard Model, a species X becomes non-relativistic during BBN, then later (necessarily if it has any effect on BBN) decays or annihilates. The effect of a non-relativistic particle cannot be described by N_ν , because the cosmic equation of state during BBN is altered [32–35] and thus requires a dedicated analysis, which is the goal of this paper. Initial work on this possibility was considered in a pair of papers [36, 37] which considered the effect of decaying particles on BBN with either entropy producing or inert decays. This question was more recently examined in the context of decaying scalar fields present at the time of BBN [38] using Alter-BBN [39]. In addition recently the effects of a non-standard expansion rate on BBN was considered in [40]. The question of equilibration of a new species during or after BBN was considered in [41]. BBN limits to some specific models were recently applied in [42–44] and the effects of entropy injection between BBN and recombination were considered in [45] and [46].

Here we take a fresh look at the question of how large a matter component with equation of state parameter $w = p/\rho = 0$ can be present during BBN. In particular, we make use of recently constructed BBN likelihood functions [7, 31] convolved with Planck likelihood chains [25]. In standard BBN cosmology, the universe is dominated by radiation, and the time-temperature relation is well known

$$\frac{1}{2t} = H = \frac{\rho_r^{1/2}}{\sqrt{3}M_P} = \left(\frac{\pi^2 g_r}{90}\right)^{1/2} \frac{T^2}{M_P}, \quad (1.1)$$

where $H = \dot{a}/a$ is the Hubble parameter, a is the cosmological scale factor, ρ_r is the total energy density in radiation, g_r is the number of relativistic degrees of freedom, and $M_P = (8\pi G_N)^{-1/2}$ is the reduced Planck mass. This leads to the convenient relation $t_s T_{\text{MeV}}^2 = 2.41/\sqrt{g_r}$ with t measured in seconds and T in MeV. These relations assume a radiation dominated universe with $w = 1/3$. The presence of a matter component beyond the standard model would alter the equation of state and the Friedmann equation becomes

$$H^2 = \frac{\rho}{3M_P^2} = \frac{\rho_r + \rho_X}{3M_P^2}, \quad (1.2)$$

where ρ_X is the energy density of the matter component. If X , with equation of state parameter, w , comes to dominate the energy density, we have $H = \frac{2}{3(1+w)}t$.

Given the change to the cosmological evolution, we recompute the production of the light elements ${}^4\text{He}$ and D/H ¹. Any amount of matter present at the time of BBN which plays a significant role in the expansion history must decay (or annihilate) in order to avoid over-closing the Universe. As such, depending on the final state decay products, either the baryon-to-photon ratio,

$$\eta = \frac{n_{\text{baryon}}}{n_\gamma} \propto (aT)^{-3}, \quad (1.3)$$

and/or the effective number of neutrinos may differ between the time of BBN and CMB decoupling. Limits on the change in these quantities was recently considered in [31]. It is also possible that the decay products directly affect the abundances through post-BBN processing [54–67]. However, we will assume that the decays of X are not hadronic and we will only consider lifetimes shorter than 10^4 s when electromagnetic decay products are scattered sufficiently to prevent nonthermal photodissociation of any light nuclides. For longer lifetimes, these nonthermal effects can lead to stronger constraints [56, 64–66].

As noted above, we make use of BBN likelihood functions (the BBN theory likelihood convolved with the observational likelihood) and convolve this with the CMB likelihood functions taken from Planck [25]. As a result we obtain a global likelihood function $\mathcal{L}(\eta, \tau_X, \xi)$, which is a function of the our three independent input parameters. Here, τ_X is the lifetime of the matter component, and $\xi = \rho_X/\rho_r$. The total likelihood can then be marginalized to produce either single or combined likelihood functions on any combination of these parameters.

In what follows, we develop our formalism in Section 2. There we define our parameter space and describe how these are implemented in our BBN calculations. In addition, we discuss the effect of decays on changes in η and the effective number of neutrino flavors,

¹We also compute the abundances of ${}^3\text{He}$ though there currently no direct method to connect observations [47] to primordial abundances [48]. We also calculate the abundance of ${}^7\text{Li}$, but here too, the observed abundances [49–52] may not be representative of primordial abundances [53].

N_ν . The observations used to construct the likelihood functions are reviewed in Section 3. In Section 4, we present the results of our BBN calculations and the resulting likelihood function $\mathcal{L}(\eta, \tau_X, \xi)$ for both cases of electromagnetic and invisible decays. A summary and comparison with previous results are given in Section 5.

2 Formalism

Standard BBN is usually defined as the theory predicting the light element abundances using *standard* nuclear physics, *standard* particle physics (implying $N_\nu = 3$) and *standard* cosmology. In this standard model, it is assumed that the Universe is described by an FRW metric and that the Universe is radiation dominated with

$$\rho_r = \frac{\pi^2}{30} \left(2 + \frac{7}{2} + \frac{7}{4} N_\nu \right) T^4, \quad (2.1)$$

at temperatures $T \gtrsim 1$ MeV. The three contributions correspond to photons, e^\pm , and neutrinos. The cosmological scale factor scales as $a \propto t^{1/2}$ and ρ_r scales as a^{-4} leading to the time-temperature relation mentioned above. The time-temperature relation dT/dt is found from combining the Friedmann equation (1.2) with the conservation of the energy momentum tensor, giving

$$\dot{\rho} + 3(1+w)H\rho = 0. \quad (2.2)$$

For a radiation dominated universe, $w = 1/3$ and we readily obtain $\rho \propto T^4 \propto a^{-4}$.

While there are many ways to go beyond the standard model (any of them), one way to modify the standard model is to introduce a new component, X , with an equation of state parameter, w_X . As noted above, the presence of a new species X affects BBN via the cosmic expansion rate as in Eq. (1.2). If our species X is decoupled, then we have separate conservation of the energy-momentum tensor of X so that $\dot{\rho}_X = 3(1+w_X)H\rho_X$ and this means that terms in X drop out of eq. (2.2). This is easily solved and the energy density of X , ρ_X scales as

$$\rho_X(a) = \rho_1 \left(\frac{a_1}{a} \right)^{3(1+w_X)}, \quad (2.3)$$

where we set the normalization by specifying ρ to be ρ_1 at $a = a_1$.

However unless the equation of state parameter, $w_X = 1/3$, the time-temperature relation is altered and two components of the energy density are coupled (through gravity) in the Friedmann equation (1.2). When X represents additional light neutrino species (for which $w = 1/3$), then the time-temperature relation is not affected, as also holds for the contributions from Standard Model neutrinos except for small heating effects. Here however we will consider cases $w_X \neq 1/3$, and so we can not in general simply recast an arbitrary beyond the standard model component in terms of additional neutrino flavors.

It will be convenient to set the normalization before nucleosynthesis begins, and we choose the time when the (standard model) radiation density is at a temperature of $T_1 = 10$ MeV. In other words, we can define a relative density parameter by

$$\rho_X = \xi \left(\frac{T_1}{T} \right)^{(1-3w_X)} \rho_r, \quad (2.4)$$

where ξ is the fraction of the SM radiation density in X at the normalization temperature, T_1 . From here onward, we will consider X to be in the form of a pressureless gas, and so we take $w_X = 0$.

In Fig. 1, we show the evolution of several components of the energy density as a function of the scale, normalized so that $a = 1$ at $T = 10$ MeV and the relative energy density is normalized so that the energy of a single neutrino is unity at $a = 1$. The baryon density (purple line) which evolves as $\rho_B \propto a^{-3}$ is unaffected by the other components. Similarly the new component with $w_x = 0$ and $\rho_X \propto a^{-3}$ (black line) runs parallel to ρ_B . At early times and on the scale displayed, the energy density in photons, ρ_γ (orange line) and the density in a single neutrino flavor (blue line) are very close (they differ by a factor of 7/8) and scale as a^{-4} . The e^\pm energy density (green curve) is 7/4 times larger than the photon density at early times. But at a temperature $T \simeq m_e$ corresponding to $t \approx 2.8$ s and $a \approx 20$, e^\pm annihilation is not accompanied by pair production and the e^\pm begins to drop off exponentially, until all of the positrons are annihilated at $t \sim 10^3$ sec. Thereafter, the density of the remaining electrons (now non-relativistic) is simply parallel to that of the baryons whose charge they balance. As the neutrinos are largely decoupled at this point, the energy density released by the annihilations goes into heating up the photons, and one clearly sees that at late times $\rho_\gamma = (8/7)(T_\gamma/T_\nu)^{4/3}\rho_\nu$, where $(T_\nu/T_\gamma)^3 = 11/4$ due to entropy conservation. This same factor is responsible for diluting the baryon-to-photon ratio given in the figure. The new matter component has been normalized to a single neutrino so that $\xi' \equiv \rho_X/\rho_{1\nu} = 0.01$, and exceeds the photon energy density when $T_\gamma \approx (43/22)\xi T_1$. As one can see, at some point, X must decay or it will continue to dominate the energy and greatly over-close the Universe. As we will see in the next section, this value of ξ was chosen as it is close to the limit imposed by the BBN calculated abundances.

It will be convenient to separate the radiation density $\rho_r = \rho_{e\gamma} + \rho_\nu$. Here the electromagnetic component of the radiation density, namely photons and e^\pm , is $\rho_{e\gamma} = \rho_\gamma + \rho_{e^\pm}$,² and $\rho_\nu = 3\rho_{1\nu}$, where the latter is the energy density of a single Standard Model neutrino, $\rho_{1\nu} = (7\pi^2/120)T_\nu^4$ and $T_\nu = (4/11)^{1/3}T$ is the neutrino temperature well after e^\pm annihilation is complete, i.e., $T \ll m_e$. The ratio of the X -matter density to a single neutrino, ξ' was defined above, and the ratio to the electromagnetic component $\rho_{e\gamma}$ is $\xi'' = \rho_X/\rho_{e\gamma}$, both defined at $T = T_1$. For convenience we summarize these measures of the X density:

$$\xi = \left. \frac{\rho_X}{\rho_{\text{rad}}} \right|_{10 \text{ MeV}}, \quad (2.5)$$

$$\xi' = \left. \frac{\rho_X}{\rho_{1\nu}} \right|_{10 \text{ MeV}} = \frac{43}{7}\xi, \quad (2.6)$$

$$\xi'' = \left. \frac{\rho_X}{\rho_\gamma} \right|_{10 \text{ MeV}} = \frac{43}{22}\xi = \frac{7}{22}\xi', \quad (2.7)$$

all of which are evaluated at $T_1 = 10$ MeV, which we choose to ensure that neutrinos are fully coupled to the plasma. In principle the total density should include dark matter and dark energy, but neither should contribute substantially at the time of BBN.

As we have just seen, the new species must decay in order to avoid over-closing the universe today (and starting structure formation too early). For example, today, the fraction of the energy density in X , relative to the critical density, $\rho_c \equiv 3H^2 M_P^2$ can be written as

$$\Omega_X = \frac{\rho_X}{\rho_c} = \xi'' \frac{T_1}{T_0} \Omega_\gamma = 2.3 \times 10^6 \xi'', \quad (2.8)$$

where we have taken the present temperature of the CMB to be 2.3×10^{-10} MeV and $\Omega_\gamma = 5.38 \times 10^{-5}$. Thus, unless ξ'' is so small that it does not affect BBN, X must decay. We

²In addition, one may include the baryon density, but because $\eta \sim 6 \times 10^{-10}$ it can be safely neglected.

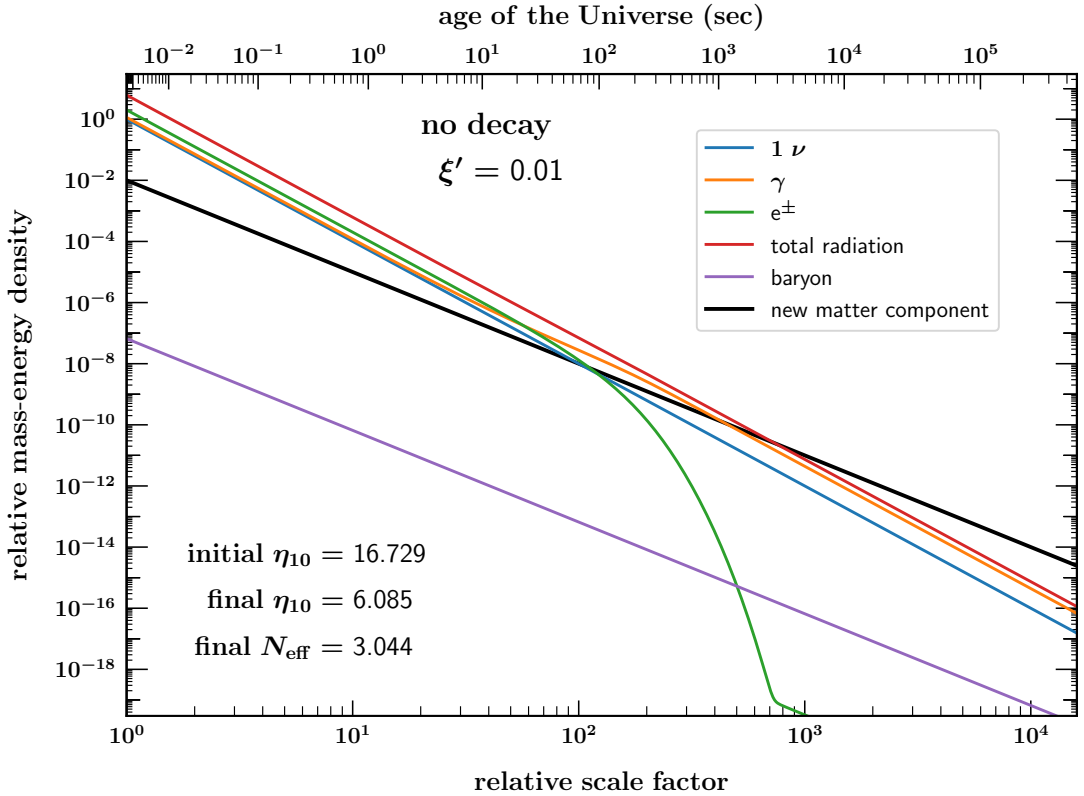


Figure 1. The evolution of the energy densities of baryons (purple line), e^\pm (green curve), photons (orange line), a single neutrino species (blue line), total radiation (red line), and a new matter component (black line). The X -energy density at $T = T_1 = 10$ MeV was set at $\xi' = 0.01$.

quantify this via a particle lifetime τ_X , and associated decay rate

$$\Gamma_X = \frac{1}{\tau_X}. \quad (2.9)$$

Allowing for decays, the equation for energy-momentum conservation is now

$$\frac{d}{dt}\rho_X + 3\frac{\dot{a}}{a}\rho_X = -\Gamma_X\rho_X, \quad (2.10)$$

and thus ρ_X evolves as

$$\rho_X = \rho_1 \left(\frac{a_1}{a}\right)^3 e^{-\Gamma_X t} \quad (2.11)$$

showing a factorization of the cosmic volume dilution and the exponential decay.

Decays will occur when the decay rate becomes comparable with the Hubble rate. It is convenient to distinguish between two possibilities: decays occur when $\rho_r > \rho_X$ or when $\rho_r < \rho_X$. In the former case, we can assume that the energy density driving the expansion is dominated by ρ_r , and we find the temperature of the radiation when decay occurs from setting $\Gamma_X = 2H$ leading to

$$T_d = \left(\frac{90}{4\pi^2 g_d}\right)^{1/4} (\Gamma_X M_P)^{1/2} = 0.86 \text{ MeV} \left(\frac{10.75}{g_d}\right)^{1/4} \left(\frac{1 \text{ sec}}{\tau_X}\right)^{1/2}, \quad (2.12)$$

where $g_d = g(T_d)$ is the number of degrees of freedom in the radiation bath at temperature T_d . While our results will not depend explicitly on the mass of X , we will assume that $m_X > T_d$ and all decays – even those to visible matter – will occur out of equilibrium. Clearly to satisfy $\rho_X < \rho_r$ at T_d , we must have $T_d > \xi T_1$ and

$$\tau_X < \left(\frac{90}{4\pi^2 g_d} \right)^{1/2} \frac{M_P}{\xi^2 T_1^2} \quad \rho_X < \rho_r \text{ @ } T = T_d. \quad (2.13)$$

Alternatively, if X decays while it dominates the energy density, decay occurs when $\Gamma_X = \frac{3}{2}H$ and

$$T_d = \left(\frac{40}{\pi^2 g_d \xi T_1} \right)^{1/3} (\Gamma_X M_P)^{2/3} = 0.46 \xi^{-1/3} \text{ MeV} \left(\frac{10.75}{g_d} \right)^{1/3} \left(\frac{1 \text{ sec}}{\tau_X} \right)^{2/3}. \quad (2.14)$$

In this case, to satisfy $\rho_X < \rho_r$ at T_d , we must have $T_d < \xi T_1$ and

$$\tau_X > \left(\frac{40}{\pi^2 g_d} \right)^{1/2} \frac{M_P}{\xi^2 T_1^2} \quad \rho_X < \rho_r \text{ @ } T = T_d. \quad (2.15)$$

Note the difference in the right hand side of Eqs. (2.13) and (2.15) is entirely due to assuming either radiation dominated in the former or matter dominated (by X) in the latter, and as such both are approximations.

All of the constraints on the matter domination can be expressed in terms of the two parameters, τ_X and ξ which characterize the model. The choice of parameters which distinguish whether the decay of X takes place in a matter dominated or radiation dominated is shown in Fig. 2. At the moment of matter and radiation equality, $H = 4(\sqrt{2} - 1)/3t$. In Fig. 2, we show the (τ_X, ξ) parameter plane. The sloped line shows the value of ξ when $\rho_X = \rho_r$ at $T = T_d$ or equivalently $t = \tau_X$. For values of ξ above the line decays occur when the Universe is dominated by the energy density of X , and values of ξ below the line have decays in a radiation dominated era. While subtle, the line is not perfectly straight and is bumped up when e^\pm annihilation occurs changing the number of degrees of freedom. The vertical arrows indicate the approximate times corresponding to neutrino decoupling (taken here to be $T = 1$ MeV) and e^\pm annihilation at $T = m_e$.

Whether or not X decays in a matter or radiation dominated period, entropy will be produced and will affect the baryon-to-photon ratio and the effective number of degrees of freedom. Thus either one or both of these quantities may differ at the BBN and CMB decoupling epochs. We consider two cases that lead to different results:

- **Case (a):** X decays to photons or other electromagnetically interacting particles, and
- **Case (b):** X decays to neutrinos or other weakly (or superweakly) interacting particles.

For case (a), we can approximate the increase in entropy from electromagnetic decays by considering the resulting reheat temperature defined by

$$\frac{g_d \pi^2}{30} T_R^4 = \frac{g_d \pi^2}{30} T_d^4 + \rho_X(T_d), \quad (2.16)$$

and the entropy increase is therefore

$$\left(\frac{T_R}{T_d} \right)^3 = \left(1 + \frac{\xi'' T_1}{T_d} \right)^{3/4}. \quad (2.17)$$

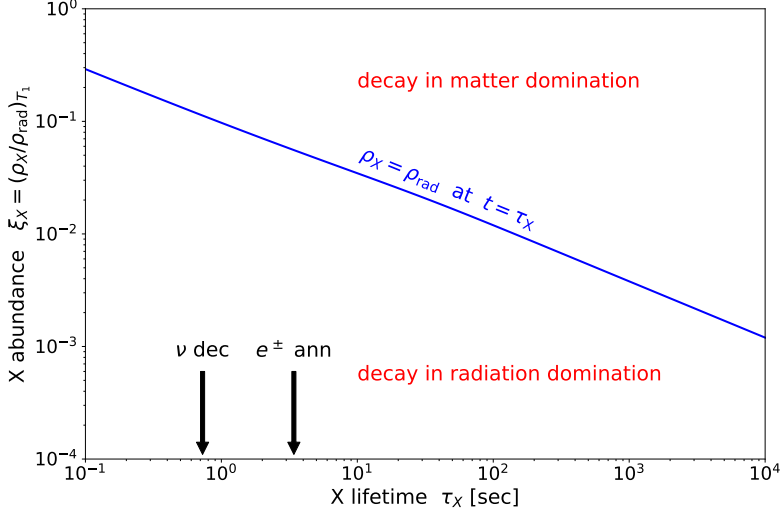


Figure 2. The $\tau_X - \xi$ parameter plane. Points above the lines have decays which occur when dominated by X , and points below have decays in a radiation dominated era. The two arrows are determined by assuming a neutrino decoupling temperature $T_{\nu\text{dec}} \simeq 1 \text{ MeV}$, and a temperature for e^\pm annihilation, $T_e \sim m_e$.

In this case, the value of η is reduced by a factor $(T_d/T_R)^3$.

$$\eta = \eta_1 \left(1 + \frac{\xi'' T_1}{T_d} \right)^{-3/4}, \quad (2.18)$$

where $\eta_1 = \eta_{10}(T_1)$ is the initial baryon-to-photon value.³ We see that the decays act to *decrease* η . We will use the CMB likelihood to constrain the *final* baryon-to-photon value. Thus as ξ'' increases, this requires a higher *initial* η_1 . This will have important consequences for the light-element abundances.

For the electromagnetic decays of case (a), the number of effective neutrinos may also be affected, depending on the temperature at which the decay occurs. For decays which occur at a temperature $T > T_{\nu\text{dec}}$, N_ν is unaffected because photons share their the decay energy and entropy with neutrinos. But for $T < T_{\nu\text{dec}}$, decays heat the photons but not the neutrinos, so that T_ν/T_γ is lower than in the standard case. The result is that N_ν is *reduced* by a factor of $(T_d/T_R)^4$. Thus

$$N_\nu = 3 \quad N_{\text{eff}} = 3.044 \quad \text{for } T_d > T_{\nu\text{dec}}, \quad (2.19)$$

$$N_\nu = 3 \left(1 + \frac{\xi'' T_1}{T_d} \right)^{-1} \quad N_{\text{eff}} = 3 \left(1 + \frac{\xi'' T_1}{T_d} \right)^{-1} + 0.044 \quad \text{for } T_e < T_d < T_{\nu\text{dec}}, \quad (2.20)$$

$$N_\nu = 3 \left(1 + \frac{\xi'' T_1}{T_d} \right)^{-1} \quad N_{\text{eff}} = 3.044 \left(1 + \frac{\xi'' T_1}{T_d} \right)^{-1} \quad \text{for } T_d < T_e, \quad (2.21)$$

and we assume $N_\nu = 3$ at $T = T_1$. It is important to note that we distinguish between N_ν and the effective number neutrinos N_{eff} . Recall that $N_{\text{eff}} > 3$ in the standard model as e^\pm

³For convenience, $\eta_{10} \equiv \eta \times 10^{10}$.

annihilation occurs before neutrinos are completely decoupled. Thus in the standard model, $N_{\text{eff}} = 3.044$ [68–72]. This is unchanged if $T_d > T_{\nu\text{dec}}$. If $T_e < T_d < T_{\nu\text{dec}}$, then the number of neutrinos is diluted but e^\pm annihilations still provide 4.4% of a neutrino. Finally when $T_d < T_e$, it is N_{eff} that is diluted.

For case b) of invisible decays, η is unaffected, and the decays into invisible particles effectively lead to an *increase* in N_ν by a factor

$$\frac{\rho_\nu + \rho_X(T_d)}{\rho_\nu} = 1 + \frac{\xi' T_1}{3T_d}, \quad (2.22)$$

if the decay occurs after neutrino decoupling. If the decay occurs before decoupling, then it matters if decays are to neutrinos, which are not invisible at this point. For decays into neutrinos no change in N_ν occurs, but η is reduced as in case (a). For decays into other invisible species (which act as radiation), N_{eff} is increased by the same factor as in Eq. (2.22). Thus for dark (non-neutrino) decays, we have

$$N_\nu = 3 \left(1 + \frac{\xi' T_1}{3T_d} \right) \quad N_{\text{eff}} = 3.044 + \frac{\xi' T_1}{T_d}. \quad (2.23)$$

and we see that N_ν *increases* due to decays, in contrast to the electromagnetic case.

The evolution of the energy densities for the two cases is shown in Fig. 3 with case (a) on the left and case b on the right. Here, we have taken $\xi' = 0.1$ and $\tau_X = 1$ s (upper), $\tau_X = 1000$ s (lower). For this value of ξ' , and we see from Fig. 2, that for the two choices of τ_X , X decays before it comes to dominate the energy density, i.e., in a radiation dominated universe for $\tau_X = 1$ s and after it starts to dominate in matter dominated universe for $\tau_X = 1000$ s. For case (a), there is a small (though non-zero) effect on the energy density of the electromagnetically interacting particles. For case b, the photon energy density is unaffected, but we see the appearance of a component of dark radiation (dashed-dotted curve). At early times, the energy density of the radiation scales as $\rho_{\text{dark}r} \propto a^{-3/2}$ (rather than a^{-4}) [73] as early decays continuously add to the energy density of the dark radiation. Once the lifetime becomes shorter than the age of the Universe, the density X drops exponentially and the density of the dark radiation redshifts as a^{-4} as might be expected.

Note that in each case considered, we adopt an initial value for $N_\nu = 3$. As discussed above, in the absence of a matter component, this leads to a final $N_{\text{eff}} = 3.044$. The effects of the matter component may decrease N_{eff} (in case a) - as seen in Eqs. (2.20) and (2.21) or increase N_{eff} (in case b) - as seen in Eq. (2.23). The final value of N_{eff} is given in each of the panels in Fig. 3. Also shown is the final value of η_{10} . These values are chosen from the likelihood analysis in the next section and the values differ for cases (a) and (b) and will be discussed below. The initial value of η (η_1), also reported in the figure, is related to this final value as approximated by Eq. (2.18) for case (a), and is unchanged in case (b), modulo the standard dilution of η due to e^\pm annihilation by the factor of (4/11).

3 Inputs: Light Element Abundances and the CMB

The constraints from BBN rely on accurate observational determinations of the light element abundances, and on cosmological parameters derived from the CMB. These are discussed in detail elsewhere, e.g., [7]; we summarize the results here.

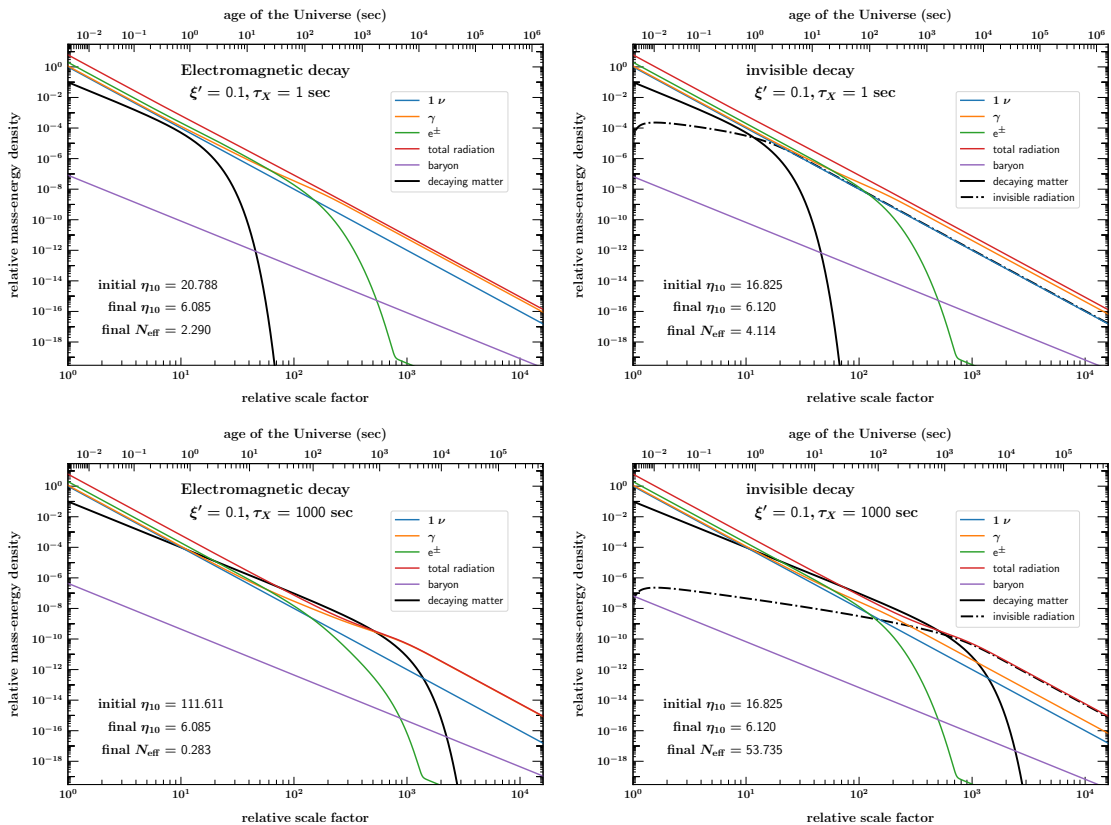


Figure 3. The evolution of the energy densities of baryons (purple line), e^\pm (green curve), photons (orange line), a single neutrino species (blue line), and a new matter component (black line). Here, $\xi' = 0.1$ with $\tau_X = 1$ s (upper) and $\tau_X = 1000$ s (lower). X decays to electromagnetically interacting particle in the left panels and to a dark component in the right panels. The dashed-dotted curve in the right panels shows the evolution of this dark component. Note that the adopted value for the final value of η_{10} is different for EM and dark decays as explained in the text. The initial value of $N_\nu = 3$ is fixed in all panels.

Deuterium is observed in high redshift quasar absorption systems [10–17], where the isotopic abundance is now determined with accuracy of approximately 1%, giving

$$\left(\frac{\text{D}}{\text{H}}\right)_{\text{obs}} = (2.55 \pm 0.03) \times 10^{-5}. \quad (3.1)$$

^4He is observed in extragalactic HII regions using a series of ^4He and H emission lines. The observational determination of ^4He has improved recently [18–23]. A recent analysis including high quality observations of the Leoncino dwarf galaxy leads to an inferred primordial abundance of [20]

$$Y_{p,\text{obs}} = 0.2448 \pm 0.0033. \quad (3.2)$$

These mean abundances with their 1σ uncertainties (assumed Gaussian) allow us to define an observational likelihood function \mathcal{L}_{obs} for ^4He and D/H. As noted earlier, though we compute the abundances of ^3He and ^7Li , we do not construct observational likelihood functions for these isotopes.

Turning to the CMB, temperature and polarization anisotropies famously encode a wealth of cosmological parameters, which depend on the cosmological model assumed. Since we consider cases where decays can change the cosmic radiation content, we are interested in models in which N_{eff} can vary. As we showed recently, these models give a baryon density or baryon-to-photon ratio, $\eta_{10} = 6.090 \pm 0.061$ based on *Planck* data alone. Furthermore, the value of N_ν is found to be $N_\nu = 2.800 \pm 0.294$.⁴ The results which include BBN will be discussed below.

4 Results

As discussed above, we have modified our BBN code to not only account for an additional component to the energy density, but also to account for the possibility that the new component has an equation of state which differs from $w = 1/3$. This results in a change in the time-temperature relation which is so crucial in the competition between the expansion time-scale and the rate for nuclear reactions. However a few comments are in order before we begin to present our constraints. First, we have noted that we consider the possibility that X decays either into products with electromagnetic interactions (case a), or into dark radiation (case b). If X decays into hadronic products which can affect directly the abundances of the light elements during or immediately after BBN, the constraints on ξ are significantly stronger and the question of matter domination during BBN becomes moot [54–63]. The change in the energy density and the time-temperature relation become irrelevant. Therefore we do not consider this possibility here. Second, so long as the lifetime of X is sufficiently low ($\tau_X \lesssim 10^4$ s), the electromagnetic decay products thermalize rapidly due to large radiation density and have a negligible effect on the post-processing of the BBN nuclei. However, for longer lifetimes, the energies of the decay products is not downgraded and post-process is again significant and very strong constraints on ξ can be derived [56, 64–66]. Therefore we do not consider lifetimes $\tau_X \gtrsim 10^4$ s for case (a). See for example [58, 61] for constraints on decaying particles with both hadronic and electromagnetic decay products.

To get an idea of the effect on the light element abundances, we show in Fig. 4 the evolution as a function of time (and temperature) of the baryonic components involved in BBN for $\xi' = 0.01$ (upper panels) and $\xi' = 1$ (lower panels) for EM decays (left panels) and dark decays (right panels) all with $\tau_X = 10$ s (though the effect of τ_X can not be seen on the scale of these plots). We see that the rapid decline in the neutron density occurs as the light elements abundances grow. For EM decays, this is delayed when the matter density is high (as in the lower left panel) due to the increased expansion rate. As a consequence, though one can not see it easily on the scale of the plot, the ${}^4\text{He}$ abundance increases slightly when the X abundance is initially large. This can be traced to the fact at higher ξ' , the initial value of η (η_1) is higher as can be seen from Eq. (2.18). The values of η_1 are given in the figure. Recall that we have fixed the final value of $\eta_{10} = 6.085$ from the likelihood analysis below. For small ξ' as in the upper left panel, the initial value of $\eta_1 = 17.941$ is similar to the standard initial value $(11/4) \times 6.085 = 16.733$. For large ξ' as in the lower left panel, the initial value of $\eta_{10} = 48.5$ and differs significantly leading to the changes in the element abundances. Since the ${}^4\text{He}$ abundance increases (logarithmically) with η , this increase in η leads to a higher helium abundance. What is more easily visible is the decrease in the D/H abundance by a factor of about 0.7 as ξ' is increased from 0.01 to 1. This is significant as the

⁴These values differ slightly from the those published in [25], which are derived from likelihood chains which assume an a priori relation between the helium abundance and the baryon density.

observational uncertainty in D/H is about 1% (see Eq. (3.1)). This drop can also be traced to the increased initial value of η as D/H decreases with increased η . The same is true for the ^3He abundance. The ^7Li abundance increases slightly, as its origin is ^7Be whose abundance increases with η . The final abundance of each of the element isotopes is collected in Table 1. As in Fig. 3, in case (a) the drop in N_{eff} . This drop is significant when ξ' is large.

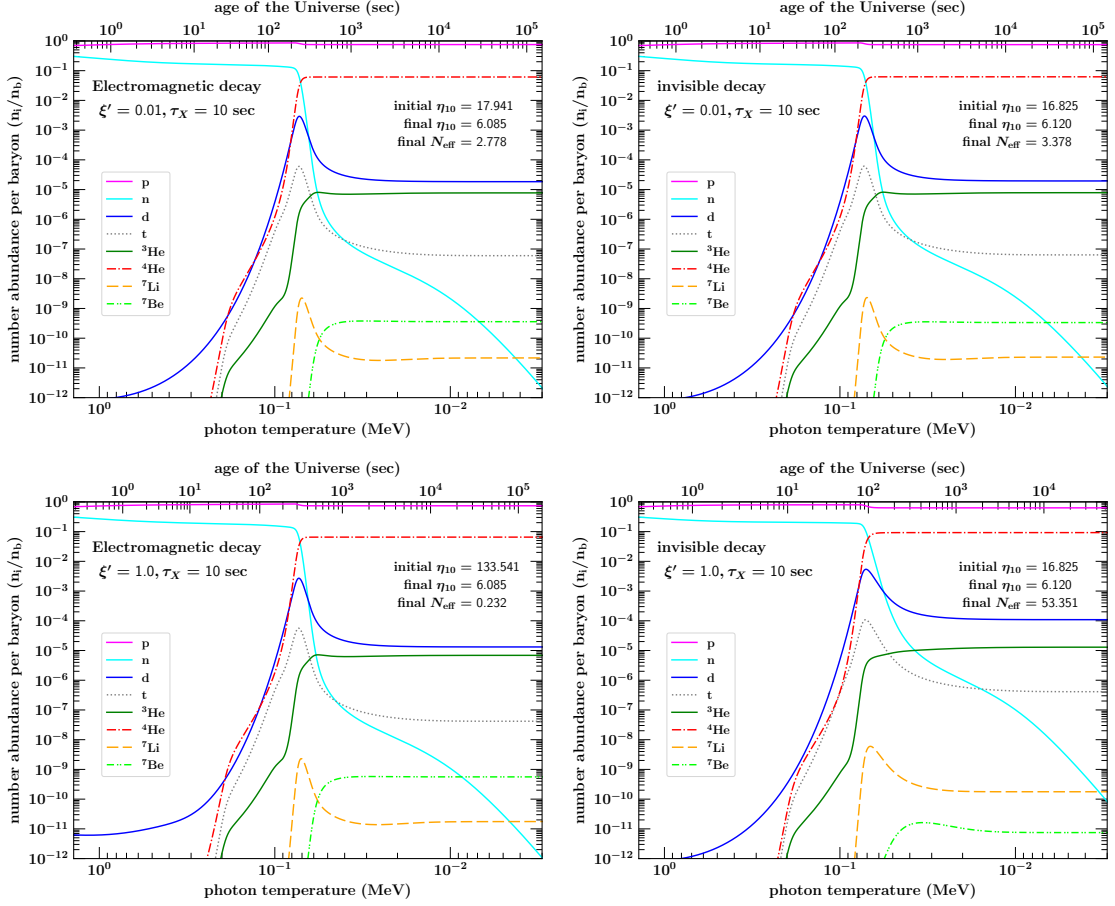


Figure 4. The evolution of the abundances of the light elements produced during BBN with $\tau_X = 10$ s and $\xi' = 0.01$ (upper), $\xi' = 1$ (lower) for EM decays (left) and dark decays (right). As in Fig. 3, the adopted final η_{10} are different for EM and dark decays.

Table 1. Final abundances of the light element isotopes in each of the cases considered in Fig. 4.

Case	EM: $\xi' = 0.01$	EM: $\xi' = 1$	Dark: $\xi' = 0.01$	Dark: $\xi' = 1$
^4He	0.2461	0.2621	0.2497	0.3713
$(\text{D}/\text{H}) \times 10^5$	2.44	1.78	2.60	17.3
$(^3\text{He}/\text{H}) \times 10^5$	1.03	0.94	1.06	2.12
$(^7\text{Li}/\text{H}) \times 10^{10}$	5.05	7.83	4.77	2.94

For completeness, we also show in Fig. 4 the abundance evolution when the X -decay

products are dark. Recall that η_{10} is unchanged in this case up to its standard model dilution, however N_{eff} increases and is significantly altered when ξ' is large as in the lower right panel of Fig. 4. This leads to the sizeable changes in the element abundances displayed in the figure.

To obtain constraints in the (η, τ_X, ξ) parameter space we construct likelihood functions for the CMB, the BBN abundances, and as noted above the observational abundances. The CMB likelihood, $\mathcal{L}_{\text{NCMB}}(\eta, N_\nu, Y_P)$ is taken from *Planck 2018* data. We use the `base_nnu_yhe_plikHM_TTTEEE_lowl_lowE_post_lensing` chains⁵ which provide the likelihoods when the number of neutrinos, N_ν , is allowed to vary. While the BBN abundances are computed here for each value of (η, τ_X, ξ) , the uncertainties stemming from the nuclear rates are taken from the Monte-Carlo analysis in [7, 31], and allows us to construct the BBN likelihood $\mathcal{L}_{\text{mBBN}}(\eta, \xi, \tau_X)$. This differs from the standard BBN likelihood as it allows for an extra matter component which affects the expansion rate and the time-temperature relation and thus evolution of the nuclear rates. As the uncertainty in the abundances are dominated by the uncertainties in the nuclear rates, they are relatively insensitive to the choice of ξ , and τ_X . Our total likelihood function comes from the convolution of the CMB, BBN and observational likelihood functions,

$$\mathcal{L}_{\text{mBBN+NCMB+obs}}(\eta, \tau_X, \xi) \propto \int \mathcal{L}_{\text{NCMB}}(\eta, N_\nu, Y_P) \mathcal{L}_{\text{mBBN}}(\vec{X}; \eta, \tau_X, \xi) \prod \mathcal{L}_{\text{obs}}(X_i) dX_i, \quad (4.1)$$

by integrating over the abundances $X_i = Y_P$ and D/H. Note that although N_ν is an argument of $\mathcal{L}_{\text{NCMB}}$, it is not an argument of the convolved likelihood function. We are assuming $N_\nu = 3$ at the onset of BBN. However, the decays of X , may affect the number of relativistic degrees of freedom parameterized as N_ν as given in Eqs. (2.19, 2.20, 2.21) and (2.23). This is used as an input to $\mathcal{L}_{\text{NCMB}}$, but it completely determined by (τ_X, ξ) .

Before we present the results of the current analysis, we recall the *standard* BBN likelihood results when N_ν is *not* fixed to be 3. When $\mathcal{L}_{\text{mBBN}}(\vec{X}; \eta, \tau_X, \xi)$ is replaced with $\mathcal{L}_{\text{NBBN}}(\vec{X}; \eta, N_\nu)$ and marginalized over the abundances of D and He, we obtain the BBN likelihood (with arguments (η, N_ν)). This results in a mean (and peak) value for $\eta_{10} = 6.088 \pm 0.054$ and a mean value for $N_\nu = 2.898 \pm 0.141$ with a peak value of $2.895_{-0.141}^{+0.142}$ [31]. While this is perfectly consistent with the Standard Model value of 3 (the 95% CL upper limit is $N_\nu < 3.18$), it does provide a slight preference for a *decrease* in N_ν as might be obtained by a component of non-relativistic matter as achieved in Eqs. (2.20) and (2.21), when $\xi \neq 0$ and $T_d < T_{\nu\text{dec}}$.

Indeed for case (a), Eqs. (2.20) and (2.21) allow us to estimate a preferred value of $\xi'' T_1 / T_d$. For a given preferred CMB value of N_ν , we can determine

$$\xi''_{\text{pref}} = \frac{3 - N_\nu T_d}{N_\nu T_1}. \quad (4.2)$$

Ignoring the weak dependence on g_d , and writing $T_d/1 \text{ MeV} \simeq (\tau_x/1 \text{ s})^{-1/2}$ as in eq. (2.12), we have roughly

$$\xi'_{\text{pref}} \sim 0.01 \left(\frac{1 \text{ s}}{\tau_X} \right)^{1/2}, \quad (4.3)$$

where we have included the factor of 22/7 to write ξ' . For case b), since we expect an increase in N_ν , the peak of the likelihood function should correspond to the Standard Model value with $\xi' = 0$ and does as we shall see below.

⁵https://wiki.cosmos.esa.int/planck-legacy-archive/index.php/Cosmological_Parameters.

4.1 Case (a): Electromagnetic Decays

We begin by discussing our results for case (a) with visible (electromagnetic) decays. Figure 5 shows likelihood contours rendered in the 3-D (η, τ_X, ξ') space. We see that the contours prefer η to be around the CMB *Planck* value. This leads to nearly planar features in (τ_X, ξ') around a relatively thin range in η . The exception is at the largest ξ' values, where the contours curve towards slightly lower values of η . This can be understood when considering the positive correlation between η and N_ν in the CMB data [25, 31]. Since large ξ' reduces N_ν it must be compensated for by lowering η . As we will see, the global maximum likelihood is in this region of somewhat reduced η . We also see that within this preferred range for η , the matter abundance is constrained to lower values as its lifetime is increased, as predicted by Eq. (4.3). This effect is clearly seen in the likelihood slices shown in Fig. 6.

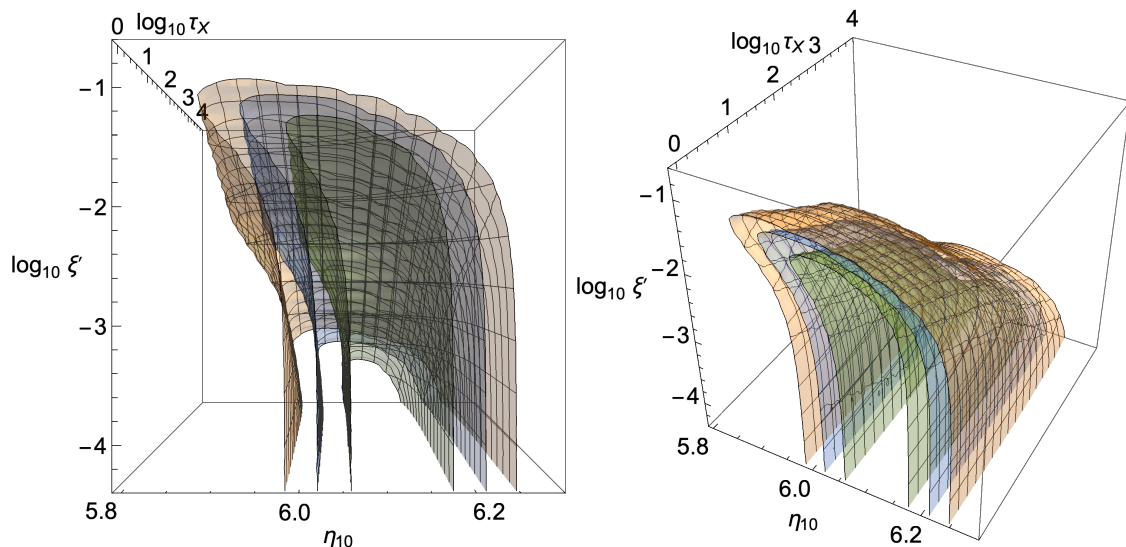


Figure 5. Likelihood contours rendered in the 3-D (η, τ_X, ξ') space. We see that the CMB-preferred η value leads to a nearly planar region of high likelihood in (τ_X, ξ') ; the walls go straight down for even lower ξ' . There is a slight shift to lower η at high ξ' , where the likelihood is maximum.

To examine the likelihood function in more detail, in Fig. 6 we show a series of likelihood plots projected onto the τ_X, ξ' plane for different values of $\eta_{10} = 5.885 - 6.285$ in increments of 0.05. Each of these corresponds to a vertical slice in Fig. 5. The peak of the likelihood function occurs at $\eta_{10} = 6.085$ (our data resolution was run at increments of 0.005 in η_{10} , so this value is essentially equivalent to the value of $\eta_{10} = 6.088$ at the peak of the SBBN likelihood function) which is shown separately in Fig. 7. Since N_ν is effectively reduced (as is preferred in SBBN with variable N_ν), it is not a surprise that the peak value of η_{10} matches the SBBN with variable N_ν value. The total likelihood function was integrated over the η, τ_X, ξ' volume. Note that to properly integrate over the volume of Fig. 5, the likelihood function was weighted by the product of $\tau_X \xi'$ with respect to the volume element in the linear-log-log space as

$$\mathcal{L} dV = \mathcal{L}(\eta, \tau_X, \xi') d\eta d\tau_X d\xi' = \mathcal{L}(\eta, \tau_X, \xi') \cdot \tau_X \xi' d\eta d\ln\tau_X d\ln\xi'. \quad (4.4)$$

This allows us to produce the iso-likelihood contours shown in the figures.

At values of $\eta_{10} \leq 5.85$ the likelihood function is near 0 for all the values of τ_X, ξ' considered and all are outside the 99% CL. Starting with the upper left panel ($\eta_{10} = 5.885$)

Electromagnetic decay : likelihood slices with confidence intervals

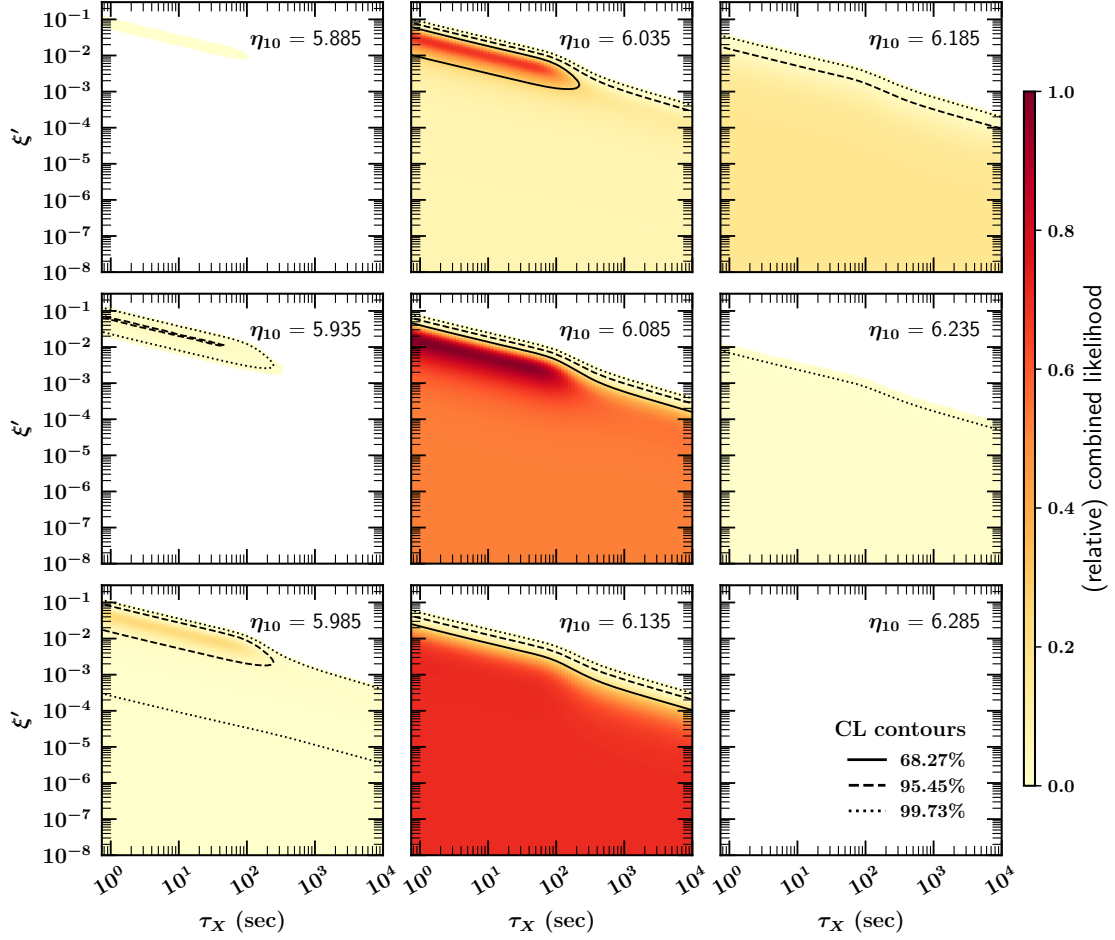


Figure 6. Likelihood contours in the (η, ξ', τ_X) space, shown as slices at fixed η . Colors denote the relative value of the likelihood function indicated by the scale at the right. The 68%, 95% and 99% CL contours are shown by solid, dashed, and dotted curves respectively.

of Fig. 6, we see evidence for a non-zero likelihood along a strip of points with $\tau_X \lesssim 100$ s though these still lie outside the 99% CL. At larger $\eta_{10} = 5.935$, the strip is expanded and is within the 99% CL contour shown by the dotted curve. A very thin strip is within the 95% CL shown by the dashed curve. Moving to larger $\eta_{10} = 5.985$, we see the non-zero likelihood extending to larger τ_X and a broadened 95% CL contour. At $\eta_{10} = 6.035$, the 68% CL contour is visible and all points with low ξ' have non-zero likelihoods. At this and higher values of η_{10} , we see that the 95% and 99% CLs are no longer closed and include the Standard Model case with $\xi' = 0$ and the position of the peak of the likelihood is becoming apparent. At $\eta_{10} = 6.07$ (not shown) even the 68% CL contour does not close. The peak of the likelihood function is seen in the middle panel and in Fig. 7, and occurs at $\eta_{10} = 6.085$, $\tau_X = 0.89$ s and $\xi' = 0.016$ and the value of the likelihood function at that point is normalized to 1. Note that at the peak, $\xi'(\tau_X/1 \text{ sec})^{1/2} = 0.015$ and the peak is very close to the left edge of the range plotted, which is $\tau_X = 0.74 - 10^4$ s where the lower limit on τ_X corresponds to decay temperatures in excess of 1 MeV. As one can see the fit is almost equally as good for any $\tau_X \lesssim 100$ s with ξ'

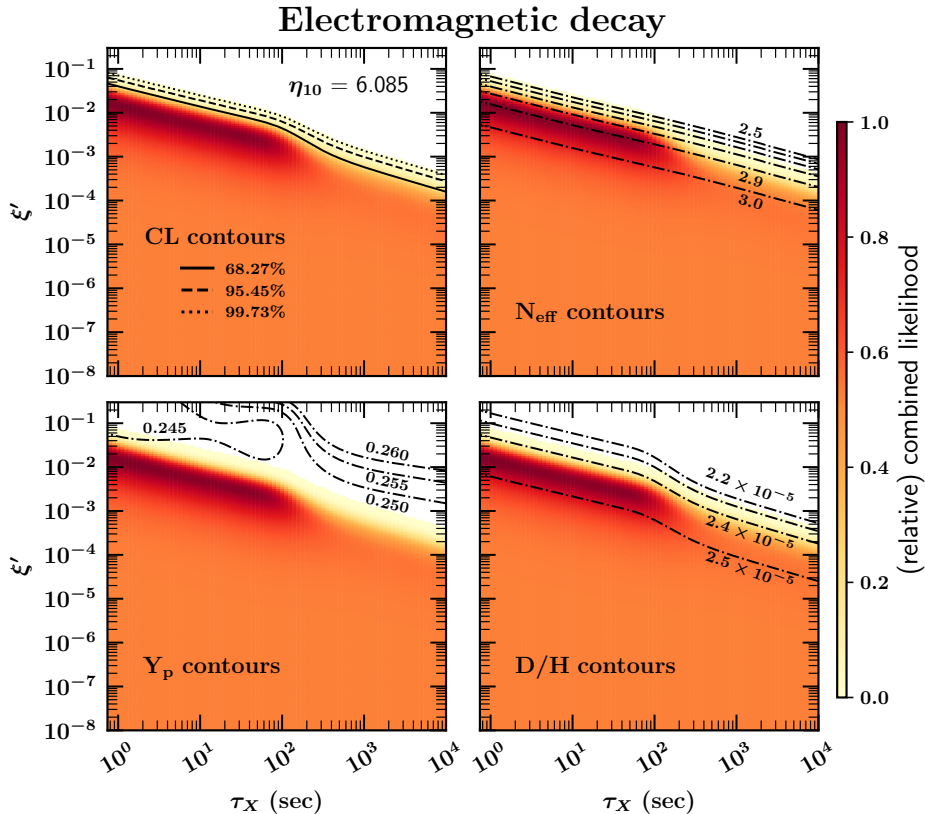


Figure 7. Contours for the EM decay case in the (τ_X, ξ') plane, evaluated at the maxim likelihood baryon-to-photon ratio $\eta_{10} = 6.085$. Dashed lines show: (a) likelihood contours, (b) N_{eff} , (c) Y_p , (d) D/H.

scaling as given in Eq. (4.3). It is important to note that at 68% CL, we have only an upper limit on ξ' (shown by the solid curve in Fig. 6) as $\xi' = 0$ (i.e. standard BBN) is consistent with the CMB and observational data. When η is increased beyond the value at the peak, as shown in the remaining panels of Fig. 6, the likelihood drops. For $\eta_{10} = 6.185$ only the 95% and 99% CLs are visible (even at low values of ξ') and both of these likelihood contours are gone at $\eta_{10} = 6.285$.

In Fig. 7, we concentrate on the peak likelihood value in the τ_X, ξ' plane along the slice at $\eta_{10} = 6.085$. In addition to the likelihood contours (upper left), we show the the effective number of relativistic degrees of freedom (upper right) and the abundances of Y_p (lower left) and D/H (lower right). As discussed previously, and exhibited analytically in Eqs. (2.19-2.21), the effective of degrees of neutrino drops below 3, as ξ' is increased (for $\xi' = 0$, we have the Standard Model value of $N_{\text{eff}} = 3.044$). We see then that the ridge including the peak likelihood aligns with $N_{\text{eff}} \simeq 2.904$ and is close to the Standard BBN best fit value of $N_\nu = 2.898$, corresponding to $N_{\text{eff}} = 2.941$; the two are slightly different because the matter component changes the expansion rate somewhat differently from radiation. As one can see, the peak of the likelihood function agrees quite well with the rough estimate given in Eq. (4.3). While one may be tempted to conclude that BBN prefers some amount of non-relativistic (unstable) matter present during nucleosynthesis, the statistical significance of this conclusion is rather weak. The abundances of ${}^4\text{He}$ and D/H are dependent on η , but

predominantly in a similar manner as in standard BBN. We have verified that ${}^7\text{Li}$ (not shown) takes standard BBN values in the allowed regions.

As noted earlier, if we fix the final value of η , then because of the dilution from X decays and given in Eq. (2.18), the value of η during BBN may be much higher, particularly for large ξ' . This accounts for the increase (decrease) in the ${}^4\text{He}$ (D/H) abundance. For the case of Y_p , we see that the abundance dips to a valley for $\tau_X \lesssim 100$ sec and $\xi' \sim 0.1 - 1$. This corresponds to decays during BBN, when the X density begins to approach the radiation density. The ${}^4\text{He}$ abundance is sensitive to both the higher initial η value, but also smaller N_{eff} value, effects which oppose each other. In the valley region, the N_{eff} effect is slightly more important.

Figure 8 show the likelihood function (4.1) marginalized over η_{10} by integrating along the η_{10} axis of Fig. 5. The result of marginalization over η is projected onto the the (τ_X, ξ') plane. As expected, we see that the contours closely follow the lines of constant $\xi' \tau_X^{1/2}$ but with different amplitudes for low vs high τ_X . For $\tau_X \lesssim 600$ sec the decays happen during BBN, and we have $\xi'(\tau_X/1\text{sec})^{1/2} \lesssim 0.05$ at 68% CL. The maximum likelihood is around $\xi'(\tau_X/1\text{sec})^{1/2} \simeq 0.015$, which is close to our estimate in eq. (4.3). Overall, the marginalization looks very similar to the slices shown in Figs. 6 and 7.

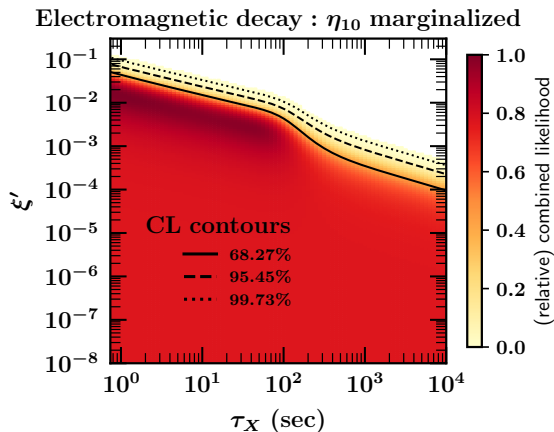


Figure 8. The likelihood function (4.1) for the EM case, marginalized over η_{10} projected onto the the (τ_X, ξ') plane.

4.2 Case (b): Invisible decays

We now turn to the case of invisible decays, where the X particle goes to neutrinos or other particles that do not interact with the plasma. As we have seen in §2, in this case the decays do not affect the baryon-to-photon ratio and do not add to the plasma entropy, and thus do not dilute N_ν as we found in the previous section. Instead, N_{eff} *increases* in this scenario, so we should not expect to find the improved fit for nonzero X density as we did for the electromagnetic decays.

Two views of the iso-likelihood function contours for a matter component with invisible decays is shown in Fig. 9. It bears several similarities with the corresponding figure for EM decays in that the likelihood contours become nearly vertical walls at low ξ' and the relation between ξ' and τ_X is maintained. At large ξ' , however the tilt towards lower η_{10} at large ξ' is absent and even tilts slightly toward higher η_{10} to compensate for the change in N_{eff} . This is

due again to the positive correlation between η and N_ν in the CMB data. The higher value of N_ν requires are (slightly) higher value of η_{10} .

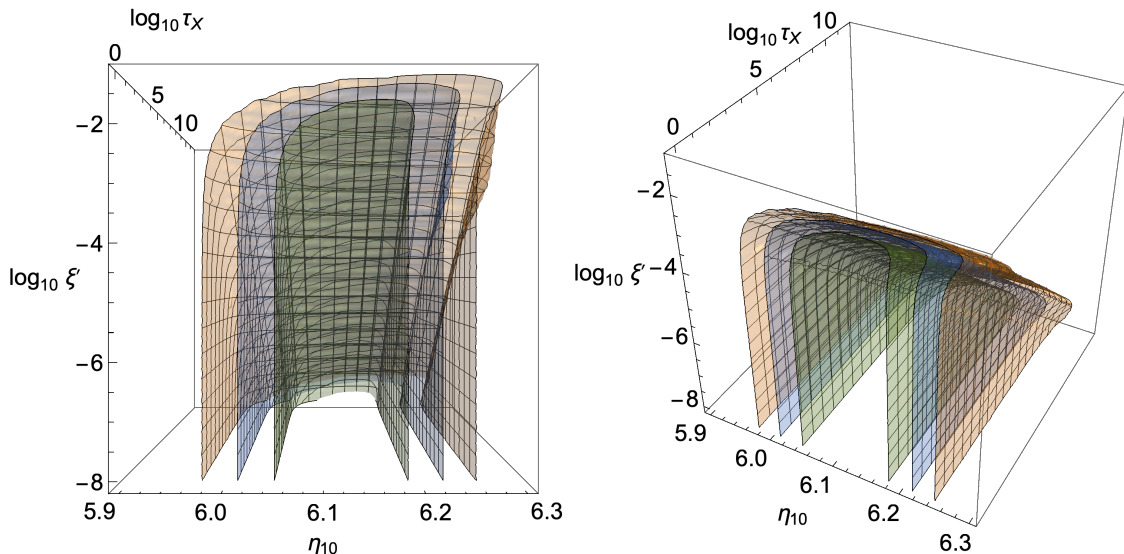


Figure 9. Likelihood contours rendered in the 3-D (η, τ_X, ξ') space for the case of dark decays. We see that the CMB-preferred η value leads to a nearly planar region of high likelihood in (τ_X, ξ') . There is a slight shift to higher η at high ξ' , where the likelihood is maximum.

Slices of this likelihood function at fixed η are shown in Fig. 10. In this case the peak of the likelihood function occurs at $\eta_{10} = 6.12$, i.e., slightly higher than in the EM-decay case, again due to the correlation between η and N_ν in the CMB data. Because these decays increase N_ν , the preferred value of ξ' is 0. In this case the final value of η resembles that of standard BBN where $\eta_{10} = 6.115 \pm 0.038$ [31]. The allowed range in η_{10} is rather narrow and the at $\eta_{10} = 5.97$ no part of the τ_X, ξ' plane is acceptable at the 99% CL. Since our results are very insensitive to ξ' and τ_X when $\xi' \ll 1$, we choose to normalize the likelihood function $\mathcal{L} = 1$ at $\xi' = 10^{-8}$ and $\tau_X = 1$ s. At $\eta_{10} = 6.02$, we see both 99% and 95% contours and the 68% CL contour appears at $\eta_{10} = 6.07$. At $\eta_{10} = 6.32$ again, no part of the plane is acceptable at even 99% CL. Note that because the decays are invisible in this case, they can not affect the light element abundances once BBN is complete. This is contrast to the case of EM decays where decays with lifetimes longer than $\sim 10^4$ s can affect the light element abundances and a different analysis is needed.

The slice at the peak value of $\eta_{10} = 6.12$ showing contours of the N_{eff} and the abundances of ${}^4\text{He}$ and D/H are shown in Fig. 11. As expected, we see the increase in N_{eff} as ξ' is increased. For Y_p we see that at small τ_X and high ξ' , the constraint roughly follows a similar slope as the N_{eff} contour. But for $\tau_X \gtrsim 100$ sec, the contour becomes horizontal, independent of ξ' . In this regime, the decays occur after BBN, and beneath the Y_p contour, the perturbations are small during BBN. Thus, nucleosynthesis proceeds as in the standard case with $N_\nu = 3$, and the light elements give the usual results. However, the decays still affect the CMB N_{eff} , which dominate the constraints in this regime. The abundance of D/H, exhibits similar behavior as Y_p . Finally, we show in Fig. 12, the likelihood plot projecton onto the τ_X, ξ' plane after marginalizing over η_{10} .

Invisible decay : likelihood slices with confidence intervals

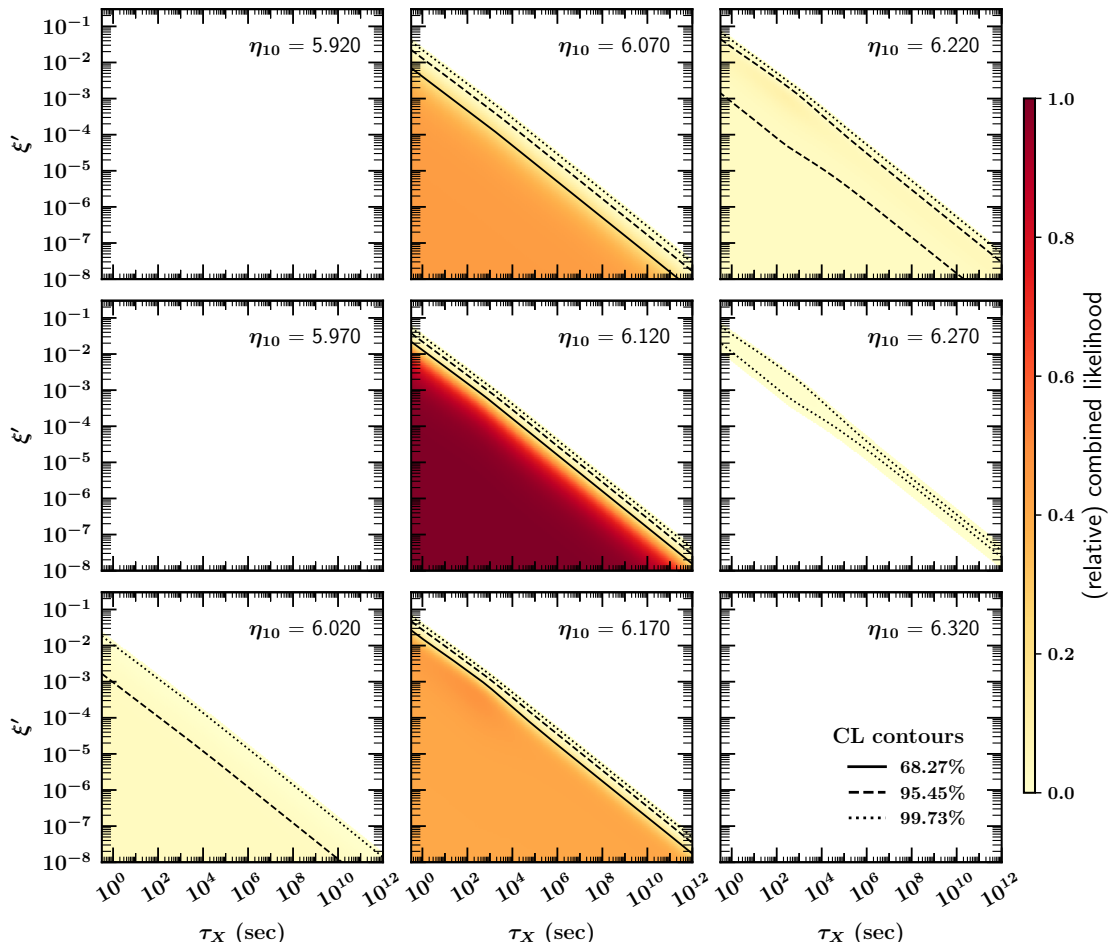


Figure 10. Likelihood contours in the (η, ξ', τ_X) space, shown as slices at fixed η for the case of dark decays. Colors denote the relative value of the likelihood function indicated by the scale at the right. The 68%, 95% and 99% CL contours are shown by solid, dashed, and dotted curves respectively.

5 Discussion

The excellent concordance between BBN theory, the observational determination of the ${}^4\text{He}$ and D/H abundances, and observations of the CMB anisotropy within the context of the standard models of particle and nuclear physics and cosmology enable us to set strong constraints on any departures from Standard Model physics. A common example of the strength of this concordance is its ability to constrain the effective number of relativistic degrees of freedom or the number of neutrino flavors. As recently shown in [31], when the number of neutrinos is allowed to deviate from its standard model value of 3, the peak BBN-CMB convolved likelihood result is $N_\nu = 2.898 \pm 0.141$.

Here we look at another relatively simple and well-motivated scenario that perturbs BBN: the presence of a species X that acts as matter and then decays out of equilibrium during or after nucleosynthesis. The presence of a matter component changes the expansion history in ways not captured by the addition of relativistic species, but if the perturbations are small we find that the net change to N_{eff} provides rather accurate insight into the constraints

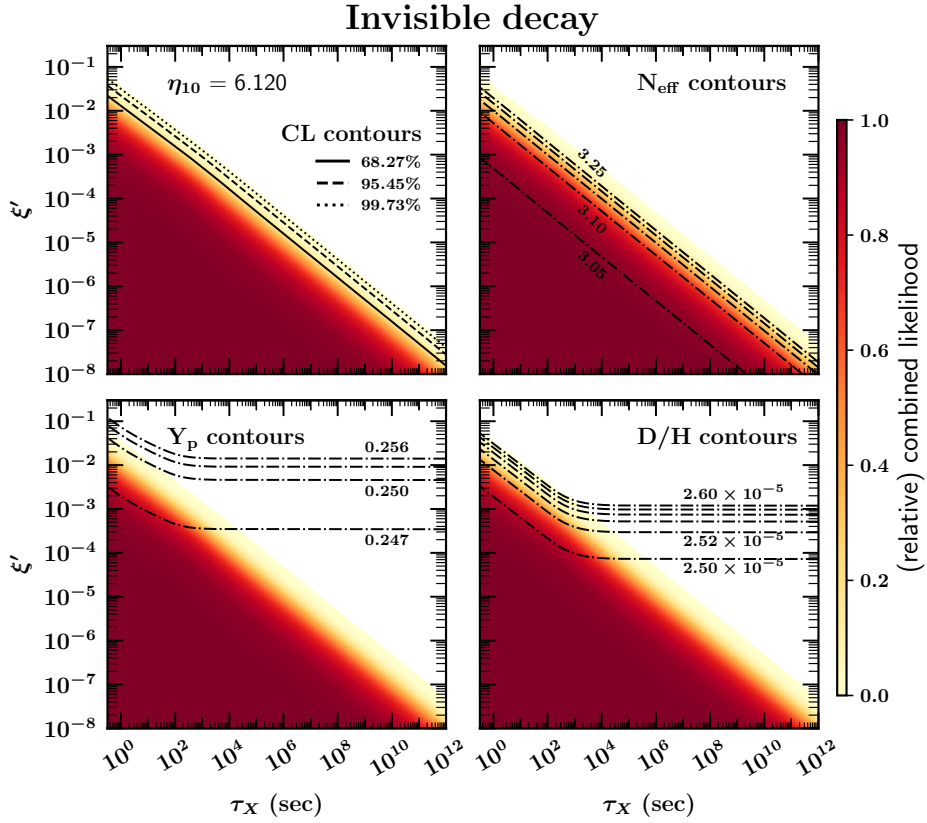


Figure 11. Contours for the case of invisible decays in the (τ_X, ξ') plane, evaluated at the maxim likelihood baryon-to-photon ratio $\eta_{10} = 6.120$. Dashes lines show: (a) likelihood contours, (b) N_{eff} , (c) Y_p , (d) D/H.

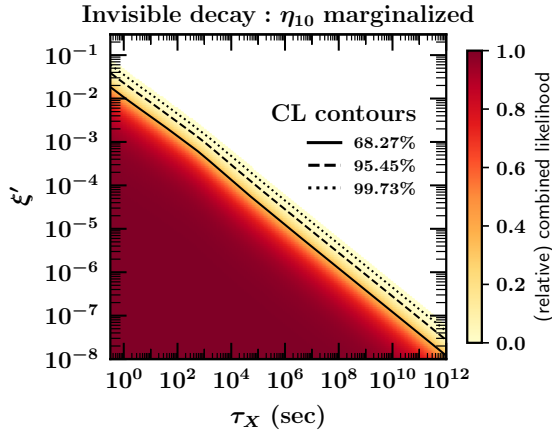


Figure 12. The likelihood function (4.1) for the invisible decays marginalized over η_{10} and projected onto the the (τ_X, ξ') plane.

posed by the light elements and the CMB.

We consider both electromagnetic as well as dark decays, which must be treated sepa-

rately. Interestingly, the electromagnetic or visible decays lead to a dilution of the neutrino energy density, and thus a decrease in N_{eff} . In addition, the decays reduce η , so that its initial value must be higher than usual in order to evolve to the CMB-preferred range. These two features combine with the mild CMB preference for $N_{\text{eff}} < 3$ to lead to a locus of nonzero perturbations giving the best fit. This regime is well-described by $\xi'(\tau_X/1 \text{ sec})^{1/2} \sim 0.015$, and $\tau_X \sim 1$ to 100 sec. To be sure, the statistical preference for this case is mild, and the standard BBN case still provides an excellent fit, with large regions of parameter space ruled out.

For the case of dark/invisible decays, the evolution of η is not perturbed, and the main effects can largely be understood in terms of changing N_{eff} . For lifetimes $\tau_X \lesssim 100$ sec, the decays occur during BBN, and the light elements place constraints competitive with the CMB N_{eff} . At larger lifetimes the light elements are unaffected during BBN, and then the CMB N_{eff} constraints dominate the limits.

We look forward to future measurements that will tighten these limits. CMB-S4 should substantially improve the precision of the CMB-determined N_{eff} [74], which as we have seen plays an important role in all of our constraints and a dominant role for EM constraints at $\tau_X \gtrsim 100$ sec. Ongoing campaigns to observe ${}^4\text{He}$ in low-metallicity dwarf galaxies can improve Y_p . Progress in this direction began with [19, 20] and is ongoing. And finally, nuclear physics measurements of the $d+d$ cross section can reduce the theoretical D/H uncertainties that currently dominate the deuterium error budget [8, 31], making it a more powerful probe of new physics.

Acknowledgments

TRIUMF receives federal funding via a contribution agreement with the National Research Council of Canada. The work of K.A.O. was supported in part by DOE grant DE-SC0011842 at the University of Minnesota.

References

- [1] T. P. Walker, G. Steigman, D. N. Schramm, K. A. Olive and H. S. Kang, *Astrophys. J.* **376** (1991) 51.
- [2] K. A. Olive, G. Steigman and T. P. Walker, *Phys. Rept.* **333**, 389 (2000) [astro-ph/9905320].
- [3] G. Steigman, *Ann. Rev. Nucl. Part. Sci.* **57**, 463 (2007) [arXiv:0712.1100 [astro-ph]].
- [4] F. Iocco, G. Mangano, G. Miele, O. Pisanti and P. D. Serpico, *Phys. Rept.* **472**, 1 (2009) [arXiv:0809.0631 [astro-ph]].
- [5] R. H. Cyburt, B. D. Fields, K. A. Olive and T.-H. Yeh, *Rev. Mod. Phys.* **88**, 015004 (2016) [arXiv:1505.01076 [astro-ph.CO]].
- [6] C. Pitrou, A. Coc, J. P. Uzan and E. Vangioni, *Phys. Rept.* **754**, 1 (2018) [arXiv:1801.08023 [astro-ph.CO]].
- [7] B. D. Fields, K. A. Olive, T. H. Yeh and C. Young, *JCAP* **03**, 010 (2020) [erratum: *JCAP* **11**, E02 (2020)] [arXiv:1912.01132 [astro-ph.CO]].
- [8] T. H. Yeh, K. A. Olive and B. D. Fields, *JCAP* **03**, 046 (2021) [arXiv:2011.13874 [astro-ph.CO]].
- [9] T. H. Yeh, K. A. Olive and B. D. Fields, *Universe* **9**, no.4, 183 (2023) [arXiv:2303.04140 [astro-ph.CO]].

- [10] M. Pettini and R. Cooke, *Mon. Not. Roy. Astron. Soc.* **425**, 2477 (2012) [arXiv:1205.3785 [astro-ph.CO]].
- [11] R. Cooke, M. Pettini, R. A. Jorgenson, M. T. Murphy and C. C. Steidel, *Ap. J.* **781**, 31 (2014) [arXiv:1308.3240 [astro-ph.CO]].
- [12] S. Riemer-Sørensen *et al.*, *Mon. Not. Roy. Astron. Soc.* **447**, 2925 (2015) [arXiv:1412.4043 [astro-ph.CO]].
- [13] S. A. Balashev, E. O. Zavarygin, A. V. Ivanchik, K. N. Telikova and D. A. Varshalovich, *Mon. Not. Roy. Astron. Soc.* **458**, no. 2, 2188 (2016) [arXiv:1511.01797 [astro-ph.GA]].
- [14] R. J. Cooke, M. Pettini, K. M. Nollett and R. Jorgenson, *Astrophys. J.* **830**, no. 2, 148 (2016) [arXiv:1607.03900 [astro-ph.CO]].
- [15] S. Riemer-Sørensen, S. Kotuš, J. K. Webb, K. Ali, V. Dumont, M. T. Murphy and R. F. Carswell, *Mon. Not. Roy. Astron. Soc.* **468**, no. 3, 3239 (2017) [arXiv:1703.06656 [astro-ph.CO]].
- [16] E. O. Zavarygin, J. K. Webb, V. Dumont, S. Riemer-Sørensen, *Mon. Not. Roy. Astron. Soc.* **477**, no. 4, 5536 (2018) [arXiv:1706.09512 [astro-ph.GA]].
- [17] R. J. Cooke, M. Pettini and C. C. Steidel, *Astrophys. J.* **855**, no. 2, 102 (2018) [arXiv:1710.11129 [astro-ph.CO]].
- [18] E. Aver, K. A. Olive and E. D. Skillman, *JCAP* **1507**, no. 07, 011 (2015) [arXiv:1503.08146 [astro-ph.CO]].
- [19] E. Aver, D. A. Berg, K. A. Olive, R. W. Pogge, J. J. Salzer and E. D. Skillman, *JCAP* **03**, 027 (2021) [arXiv:2010.04180 [astro-ph.CO]].
- [20] E. Aver, D. A. Berg, A. S. Hirschauer, K. A. Olive, R. W. Pogge, N. S. J. Rogers, J. J. Salzer and E. D. Skillman, *Mon. Not. Roy. Astron. Soc.* **510**, no.1, 373-382 (2022) [arXiv:2109.00178 [astro-ph.GA]].
- [21] T. Hsyu, R. J. Cooke, J. X. Prochaska and M. Bolte, *Astrophys. J.* **896**, no.1, 77 (2020) [arXiv:2005.12290 [astro-ph.GA]].
- [22] O. A. Kurichin, P. A. Kislitsyn, V. V. Klimenko, S. A. Balashev and A. V. Ivanchik, *Mon. Not. Roy. Astron. Soc.* **502**, no.2, 3045-3056 (2021) [arXiv:2101.09127 [astro-ph.CO]].
- [23] M. Valerdi, A. Peimbert, and M. Peimbert *Mon. Not. Roy. Astron. Soc.* **505**, no.3, 3624-3634 (2021) [arXiv:2105.12260 [astro-ph.CO]].
- [24] D. N. Spergel *et al.* [WMAP], *Astrophys. J. Suppl.* **148**, 175-194 (2003) [arXiv:astro-ph/0302209 [astro-ph]].
- [25] N. Aghanim *et al.* [Planck Collaboration], *Astron. Astrophys.* **641** (2020), A6 [arXiv:1807.06209 [astro-ph.CO]].
- [26] S. Sarkar, *Rept. Prog. Phys.* **59**, 1493-1610 (1996) [arXiv:hep-ph/9602260 [hep-ph]].
- [27] R. H. Cyburt, B. D. Fields, K. A. Olive and E. Skillman, *Astropart. Phys.* **23**, 313-323 (2005) [arXiv:astro-ph/0408033 [astro-ph]].
- [28] M. Pospelov and J. Pradler, *Ann. Rev. Nucl. Part. Sci.* **60**, 539-568 (2010) [arXiv:1011.1054 [hep-ph]].
- [29] G. Mangano and P. D. Serpico, *Phys. Lett. B* **701**, 296-299 (2011) [arXiv:1103.1261 [astro-ph.CO]].
- [30] K. M. Nollett and G. P. Holder, [arXiv:1112.2683 [astro-ph.CO]].
- [31] T. H. Yeh, J. Shelton, K. A. Olive and B. D. Fields, *JCAP* **10**, 046 (2022) [arXiv:2207.13133 [astro-ph.CO]].

- [32] E. W. Kolb, M. S. Turner and T. P. Walker, Phys. Rev. D **34**, 2197 (1986)
- [33] M. Kaplinghat, G. Steigman, I. Tkachev and T. P. Walker, Phys. Rev. D **59**, 043514 (1999) [arXiv:astro-ph/9805114 [astro-ph]].
- [34] M. Kaplinghat, G. Steigman and T. P. Walker, Phys. Rev. D **61**, 103507 (2000) [arXiv:astro-ph/9911066 [astro-ph]].
- [35] S. M. Carroll and M. Kaplinghat, Phys. Rev. D **65**, 063507 (2002) [arXiv:astro-ph/0108002 [astro-ph]].
- [36] R. J. Scherrer and M. S. Turner, Astrophys. J. **331**, 19-32 (1988)
- [37] R. J. Scherrer and M. S. Turner, Astrophys. J. **331**, 33-37 (1988)
- [38] A. Arbey and J. F. Coupechoux, JCAP **11**, 038 (2019) [arXiv:1907.04367 [astro-ph.CO]].
- [39] A. Arbey, J. Auffinger, K. P. Hickerson and E. S. Jenssen, Comput. Phys. Commun. **248**, 106982 (2020) [arXiv:1806.11095 [astro-ph.CO]].
- [40] D. Aristizabal Sierra, S. Gariazzo and A. Villanueva, JCAP **12**, 020 (2023) [arXiv:2308.15531 [astro-ph.CO]].
- [41] A. Berlin, N. Blinov and S. W. Li, Phys. Rev. D **100**, no.1, 015038 (2019) [arXiv:1904.04256 [hep-ph]].
- [42] P. D. Serpico and G. G. Raffelt, Phys. Rev. D **70**, 043526 (2004) [arXiv:astro-ph/0403417 [astro-ph]].
- [43] P. F. Depta, M. Hufnagel, K. Schmidt-Hoberg and S. Wild, JCAP **04**, 029 (2019) [arXiv:1901.06944 [hep-ph]].
- [44] S. Chang, S. Ganguly, T. H. Jung, T. S. Park and C. S. Shin, [arXiv:2401.00687 [hep-ph]].
- [45] A. C. Sobotka, A. L. Erickcek and T. L. Smith, Phys. Rev. D **107**, no.2, 023525 (2023) [arXiv:2207.14308 [astro-ph.CO]].
- [46] A. C. Sobotka, A. L. Erickcek and T. L. Smith, [arXiv:2312.13235 [astro-ph.CO]].
- [47] T. M. Bania, R. T. Rood, and D. S. Bania, Nature **415**, 54 (2002).
- [48] E. Vangioni-Flam, K. A. Olive, B. D. Fields and M. Casse, Astrophys. J. **585**, 611-616 (2003) [arXiv:astro-ph/0207583 [astro-ph]].
- [49] L. Sbordone, P. Bonifacio, E. Caffau, H.-G. Ludwig, N. T. Behara, J. I. G. Hernandez, M. Steffen and R. Cayrel *et al.*, Astron. Astrophys. **522**, A26 (2010) [arXiv:1003.4510 [astro-ph.GA]].
- [50] P. Bonifacio, L. Sbordone, E. Caffau, H. G. Ludwig, M. Spite, J. I. G. Hernandez and N. T. Behara, Astron. Astrophys. **542**, A87 (2012) [arXiv:1204.1641 [astro-ph.GA]].
- [51] D. S. Aguado, J. I. G. Hernández, C. Allende Prieto and R. Rebolo, Astrophys. J. Lett. **874**, L21 (2019) [arXiv:1904.04892 [astro-ph.SR]].
- [52] A. M. Matas Pinto, M. Spite, E. Caffau, P. Bonifacio, L. Sbordone, T. Sivarani, M. Steffen, F. Spite, P. François, and P. Di Matteo, Astron. Astrophys. **654**, A170 (2021) [arXiv:2110.00243 [astro-ph.SR]].
- [53] B. D. Fields and K. A. Olive, JCAP **10**, 078 (2022) [arXiv:2204.03167 [astro-ph.GA]].
- [54] M. Kawasaki and T. Moroi, Prog. Theor. Phys. **93**, 879 (1995) [hep-ph/9403364].
- [55] M. Kawasaki, K. Kohri and T. Moroi, Phys. Rev. D **63**, 103502 (2001) [hep-ph/0012279];
- [56] R. H. Cyburt, J. Ellis, B. D. Fields and K. A. Olive, Phys. Rev. D **67**, 103521 (2003) [astro-ph/0211258].
- [57] K. Jedamzik, Phys. Rev. D **70** (2004) 063524 [arXiv:astro-ph/0402344];

- [58] M. Kawasaki, K. Kohri and T. Moroi, Phys. Rev. D **71**, 083502 (2005) [arXiv:astro-ph/0408426 [astro-ph]].
- [59] M. Kawasaki, K. Kohri, T. Moroi and A. Yotsuyanagi, Phys. Rev. D **78**, 065011 (2008) [arXiv:0804.3745 [hep-ph]].
- [60] K. Jedamzik and M. Pospelov, New J. Phys. **11**, 105028 (2009) [arXiv:0906.2087 [hep-ph]].
- [61] R. H. Cyburt, J. Ellis, B. D. Fields, F. Luo, K. A. Olive and V. C. Spanos, JCAP **0910**, 021 (2009) [arXiv:0907.5003 [astro-ph.CO]].
- [62] V. Poulin and P. D. Serpico, Phys. Rev. Lett. **114**, no. 9, 091101 (2015) [arXiv:1502.01250 [astro-ph.CO]].
- [63] M. Kawasaki, K. Kohri, T. Moroi and Y. Takaesu, Phys. Rev. D **97**, no. 2, 023502 (2018) [arXiv:1709.01211 [hep-ph]].
- [64] M. Hufnagel, K. Schmidt-Hoberg and S. Wild, JCAP **11**, 032 (2018) doi:10.1088/1475-7516/2018/11/032 [arXiv:1808.09324 [hep-ph]].
- [65] M. Kawasaki, K. Kohri, T. Moroi, K. Murai and H. Murayama, JCAP **12**, 048 (2020) doi:10.1088/1475-7516/2020/12/048 [arXiv:2006.14803 [hep-ph]].
- [66] P. F. Depta, M. Hufnagel and K. Schmidt-Hoberg, JCAP **04**, 011 (2021) doi:10.1088/1475-7516/2021/04/011 [arXiv:2011.06519 [hep-ph]].
- [67] J. R. Alves, L. Angel, L. Guedes, R. M. P. Neves, F. S. Queiroz, D. R. da Silva, R. Silva and Y. Villamizar, [arXiv:2311.07688 [hep-ph]].
- [68] K. Akita and M. Yamaguchi, JCAP **08**, 012 (2020) [arXiv:2005.07047 [hep-ph]].
- [69] J. J. Bennett, G. Buldgen, P. F. De Salas, M. Drewes, S. Gariazzo, S. Pastor and Y. Y. Y. Wong, JCAP **04**, 073 (2021) [arXiv:2012.02726 [hep-ph]].
- [70] M. Escudero Abenza, JCAP **05**, 048 (2020) [arXiv:2001.04466 [hep-ph]].
- [71] J. Froustey, C. Pitrou and M. C. Volpe, JCAP **12**, 015 (2020) doi:10.1088/1475-7516/2020/12/015 [arXiv:2008.01074 [hep-ph]].
- [72] M. Cielo, M. Escudero, G. Mangano and O. Pisanti, Phys. Rev. D **108**, no.12, L121301 (2023) [arXiv:2306.05460 [hep-ph]].
- [73] R. J. Scherrer and M. S. Turner, Phys. Rev. D **31**, 681 (1985)
- [74] K. Abazajian, G. Addison, P. Adshead, Z. Ahmed, S. W. Allen, D. Alonso, M. Alvarez, A. Anderson, K. S. Arnold and C. Baccigalupi, *et al.* [arXiv:1907.04473 [astro-ph.IM]].